Formability Analysis of Pre-strained AA5754-O Sheet Metal Using Yld96 Plasticity Theory: Role of Amount and Direction of Uni-axial Pre-strain

S. Dhara[a], S. Basak[a], S. K. Panda[a,*], S. Hazra[b], B. Shollock[b], R. Dashwood[c]

[a]Department of Mechanical Engineering, Indian Institute of Technology Kharagpur, 721302, India
[b]Warwick Manufacturing Group, University of Warwick, Coventry, CV4 7AL, UK
[c]Coventry University, Coventry, CV1 5FB, UK

Abstract

Automotive industries are very much interested in formability of different pre-strained aluminum alloy sheets in the context of multistage stamping to fabricate complex components. In the present work, different uni-axial pre-strains of 6.4% and 12.2% were induced in AA5754-O aluminum alloy both along rolling direction (RD) and transverse direction (TD). The true stress-strain response, limiting dome height (LDH) and strain based forming limit diagram (ε-FLD) of as received and all pre-strained materials were evaluated experimentally. The anisotropy constitutive material model was developed using the Yld96 plasticity theory in-conjunction with the Hollomon isotropic hardening law to predict the yield strength evolution of the pre-strained materials. Also, it was found that the limiting strains in ε-FLD shifted significantly depending on the amount and direction of uni-axial pre-strain. Hence, the limiting strains of the as-received materials were transposed into stress space to estimate the stress based forming limit diagram (σ-FLD) using the anisotropy constitutive material model. Further, the dynamic shifts of ε-FLDs of four different pre-strained materials were predicted by successfully decoupling the σ-FLD of as-received materials within root mean square error of 0.008. Finite element models of both uni-axial pre-straining and subsequent LDH tests were developed, and the forming behavior of the pre-strained materials were predicted implementing the Yld96 plasticity model and estimated σ-FLD. It was found that LDH was significantly influenced by the amount of pre-strain, and the maximum thinning location shifted close to pole in the case of 12.2% pre-strained materials. However, the effect of uni-axial pre-strain direction on both LDH and maximum thinning location in AA5754-O material was very negligible.

Keywords – *AA5754-O; Uni-axial pre-strain; Forming limit diagram; Limiting dome height; Yld96 anisotropic yield theory; Finite element model.*

Abbreviations: σ-FLD, stress based forming limit diagram; ε-FLD, strain based forming limit diagram; UT, uni-axial tensile test; UP, uni-axial pre-strain; SC, stack compression test; UTS, ultimate tensile strength; YS, yield strength; LDH, limiting dome height.

[*]***Corresponding author***
Sushanta Kumar Panda
Associate Professor, Department of Mechanical Engineering
Indian Institute of Technology Kharagpur, West Bengal, India-721302
email: sushanta.panda@mech.iitkgp.ernet.in
Phone: +91-3222-282910, Fax : +91-3222-255303

1 Introduction

The automotive industries are very much interested in stamping of body panels, chassis and different structures using advanced high strength steels, aluminum and magnesium alloys to meet the constant increasing demand of reducing vehicle weight. Among all these materials, the non-heat treatable AA5754-O (O-annealed condition) is a suitable candidate for stamping of three dimensional complex body panels because of its light weight, high strength to weight ratio, corrosion resistance properties and recyclability. In this context, there were previous literatures available on laboratory scale simulative tests of different aluminum thin sheets such as limiting drawing ratio [1], limiting dome height [2], Erichsen cupping [3], hole flangeability [4] and V-bending and spring back [5] tests. Researchers had carried out extensive studies to understand the effect of different tool design and process parameters such as punch corner radius, die corner radius, blank holding force, temperature, strain rate and friction and lubrications [6-10]. Also, different aluminum alloy sheets were deformed under different possible strain paths ranging from tension-compression to tension-tension deformation modes to evaluate the forming limit diagram (FLD or strain based forming limit diagram or ε-FLD) [11, 12]. The detailed procedures to evaluate the ε-FLDs experimentally were discussed in different previous literatures [13, 14]. Moreover, cost effective theoretical models were also proposed to compute the limiting strains of aluminum alloys, and the two mostly used models were Marciniak-Kuczynski (M-K) [15] and Storen-Rice [16] model. Further, different anisotropy plasticity theories with strain and strain rate hardening models were implemented in these two models to predict the effect of various material parameters on the limiting strains in ε-FLD [17-19]. It was found that the limiting strains increased with the increase of sheet thickness [20], strain hardening exponent (*n*-value) [20] and strain rate sensitive index (*m*-value) [21]. Also, the sheet metal may have local nonhomogeneity due to the variations in thickness, grain size and orientation, residual stress, roughness, porosity, inclusions and second-phase particles. This local nonhomogeneity was modeled as a narrow groove to estimate the limiting strain, and it was found that the forming limit decreased with increase in nonhomogeneity within the sheet material [22]. The higher Lankford anisotropy parameter (*r*-value) had a favorable effect on the limit strain particularly in the left hand side of ε-FLD (i.e. in tension-compression deformation mode) [20]. It was also observed that weld conditions influenced the limiting strains of laser-welded blanks [23].

However, it was mentioned that *r*-value had an influence of formability during hydraulic bulge test [24]. Hence, the evaluation of these material properties and correlating these with ε-FLD were very important laboratory studies to gain the confidence of automotive industries while selecting suitable light-weight materials.

Though ε-FLD is extensively used as formability measure of sheet metals, it has been reported that the limiting strains shifted dynamically depending on the type and the amount of pre-strain in different ferrous and non-ferrous materials [25]. Graf and Hosford [26] carried out extensive experiments to evaluate ε-FLDs of tension-tension, tension-compression and plane strain pre-strained Al 2008 T4 aluminum alloy and concluded that the forming limits of uni-axial pre-strained materials were drastically changed depending on the direction of pre-strain with respect to rolling direction (RD). The limiting strain decreased when the direction of uni-axial pre-strain was parallel to RD, but the pre-straining along transverse to rolling direction (TD) increased the forming limits. It is very important to determine the limiting strains of different pre-strained materials while selecting sheet material. But the tedious testing procedures demand much time, energy and materials to evaluate ε-FLDs of pre-strained materials at each stage Therefore, several researchers [27-29] characterized the forming limits using stress-based FLD (σ-FLD), where the limiting major and minor stresses were estimated through transforming the limiting strains into stress space using suitable anisotropic yield theory, hardening law and flow rule. Stoughton [27] converted the ε-FLDs of as-received and pre-strained materials reported by Graf and Hosford [26] to stress space, and it was found that all the σ-FLDs merged very closely. Recently, Basak et al. [30, 31] estimated the strain path independent σ-FLD of Al 2008 T4 sheets using the Barlat-89 anisotropy plasticity theory and Swift hardening law, and further the formability of bi-axial pre-strained DP600 and IF steel sheets were predicted successfully implementing in finite element model.

It is noteworthy that auto-body panels were stamped using rigid dies and punches mounted in a double action hydraulic press, and the final critical shapes were obtained in multiple stages. Hence, it is very imperative to evaluate the formability of AA5754 alloy using laboratory scale simulative tests before actual stamping of the light weight components. In the present work, the effect of uni-axial pre-strain on the tensile properties and forming limit of AA5754-O was investigated. The pre-strain was induced both along RD and TD, and subsequently out-of-plane

stretch forming test (or limiting dome height test) was conducted to evaluate the formability in-terms limiting dome height (LDH) and ε-FLD. Moreover, the σ-FLD was estimated using the Yld96 anisotropy plasticity theory in-conjunction with the Hollomon hardening law. The numerical simulation of the out-of-plane stretch forming operation was carried out incorporating the pre-strain histories using LS-DYNA 971 explicit dynamic solver, and the estimated σ-FLD was implemented successfully as a damage model to predict the forming behavior of pre-strained materials.

2 Experimental details

In the present work, 1.54 mm thick AA5754-O aluminum alloy sheets were selected and the chemical composition is shown in Table 1. It was found that magnesium was the main alloying element of this non-heat treatable alloy, which imparted strength by impeding the movement of dislocations during plastic deformation. Automotive industries are interested in this alloy for fabrications of light weight auto-body panels, and hence the effect of pre-strain on the formability was investigated adopting the following detailed procedures.

Table 1 Chemical compositions of the AA5754-O alloy (weight in %) used in the present study

Al	Mg	Mn	Fe	Si	Cr	Zn	Ti	Cu
Balance	2.6-3.6	0.5	0.4	0.4	0.3	0.2	0.15	0.1

2.1 Uni-axial pre-straining

One pair of rectangular grippers were designed and fabricated in-house to clamp 105 mm$\times$500 mm sheet specimens both at the top and bottom. The fabricated grippers with the experimental set-up to impart pre-strain are shown in Fig. 1. These grippers consisted of 105 mm$\times$85 mm plates with 10 mm diameter cylindrical drawbeads press fitted at the middle. The AA5754-O alloy sheets were tightly clamped using these grippers by applying sufficient holding pressure laterally, and the uni-axial pre-strain was imparted using Zwick/Roell$\pm$250 kN fatigue test machine. The amount of pre-strain was measured in-situ by 50 mm extensometer and the required travel of the grippers was accessed by developing FE model. Accordingly four different types of pre-strain within the limit of uniform deformation region of stress-strain response were induced by deforming both along RD and TD at a cross head speed of 2 mm/min (approximately 0.011 s^{-1}), and these were: 6.4% along RD, 6.4% along TD, 12.2% along RD and 12.2% along

TD. Henceforward, these above pre-strained materials were designated as 6.4% RD, 6.4% TD, 12.2% RD and 12.2% TD respectively. To confirm the uniform strain distribution along the length of the panel, the pre-straining experiment was modeled and simulated in FE solver, LS-DYNA (discussed in section 4). It was observed from the strain contour distribution along the length of the AA5754 panel that the strain distribution on the AA5754 panel was uniform within an error of ±0.5%. The dimension of the rectangular specimens to impart pre-strain was decided considering the further fabrications of tensile, stack compression and LDH specimens from the uniform plastic strain region. The complete testing process sequence adopted in the present study is depicted in Fig. 2.

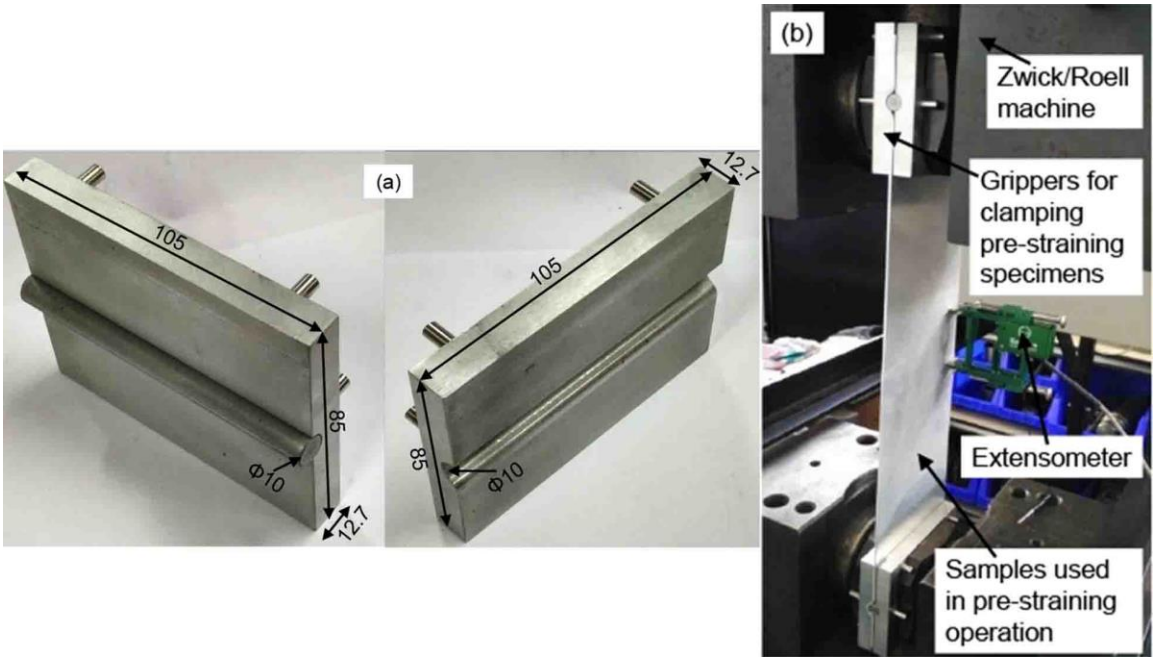

Fig. 1 Experimental set-up used for uni-axial pre-straining operation: (a) grippers used (all dimensions are in mm) and (b) clamping of specimens both at top and bottom with extensometer

2.2 Uni-axial tensile tests

Uni-axial tensile specimens were cut from as-received sheets along RD, 45° to RD (diagonal direction, DD) and TD by using wire cut electric discharge machining process. After two different amount of uni-axial pre-straining of 6.4 % and 12.2 % along RD and TD, the uni-axial tensile specimens were cut as shown in Fig. 2(b) and (c). The dimension of a tensile specimen is shown in Fig. 2(c). All the tensile tests of as received and pre-strained materials were conducted at a quasi-static crosshead speed of 2 mm/min to evaluate the yield strength (YS), ultimate tensile strength (UTS), Lankford anisotropy parameter (*r*-value), uniform elongation and total

elongation in all the three directions with respect to RD. The true stress and true strain data obtained after tensile test were fitted to Hollomon hardening law, $\bar{\sigma} = K\bar{\varepsilon}^{n}$. ASTM E517 standard [32] was followed to determine the r-value of AA5754-O material. According to the standard, the tensile specimen was axially pulled until it stretched beyond the yield point elongation but not exceeding the true strain corresponding to UTS. It was observed that, if the cut off true strain was nearer to the yield point strain then the inaccuracy in measurement was higher. Hence, the cut off true strain was kept nearer to UTS (i.e. approximately 70% of the UTS) for better accuracy and measurement ease of the anisotropic value (r-value) for both as-received and pre-strained materials. Further, the *r*-values were evaluated at any angle (θ) with respect to RD by evaluating the plastic strain ratio as shown in the Eq. (1). In the present work, plastic anisotropic parameter r_0, r_{45} and r_{90} were evaluated experimentally.

$$r_\theta = \frac{d\varepsilon_{90+\theta}}{d\varepsilon_{zz}} = -\left(\frac{d\varepsilon_{90+\theta}}{d\varepsilon_{90+\theta} + d\varepsilon_\theta}\right) \tag{1}$$

Where, r_θ = Lankford anisotropy parameter at an angle θ with respect to RD, $d\varepsilon_\theta$ = strain along an angle θ with respect to RD, $d\varepsilon_{90+\theta}$ = strain along an angle 90+θ with respect to RD and $d\varepsilon_{zz}$ = strain along thickness direction.

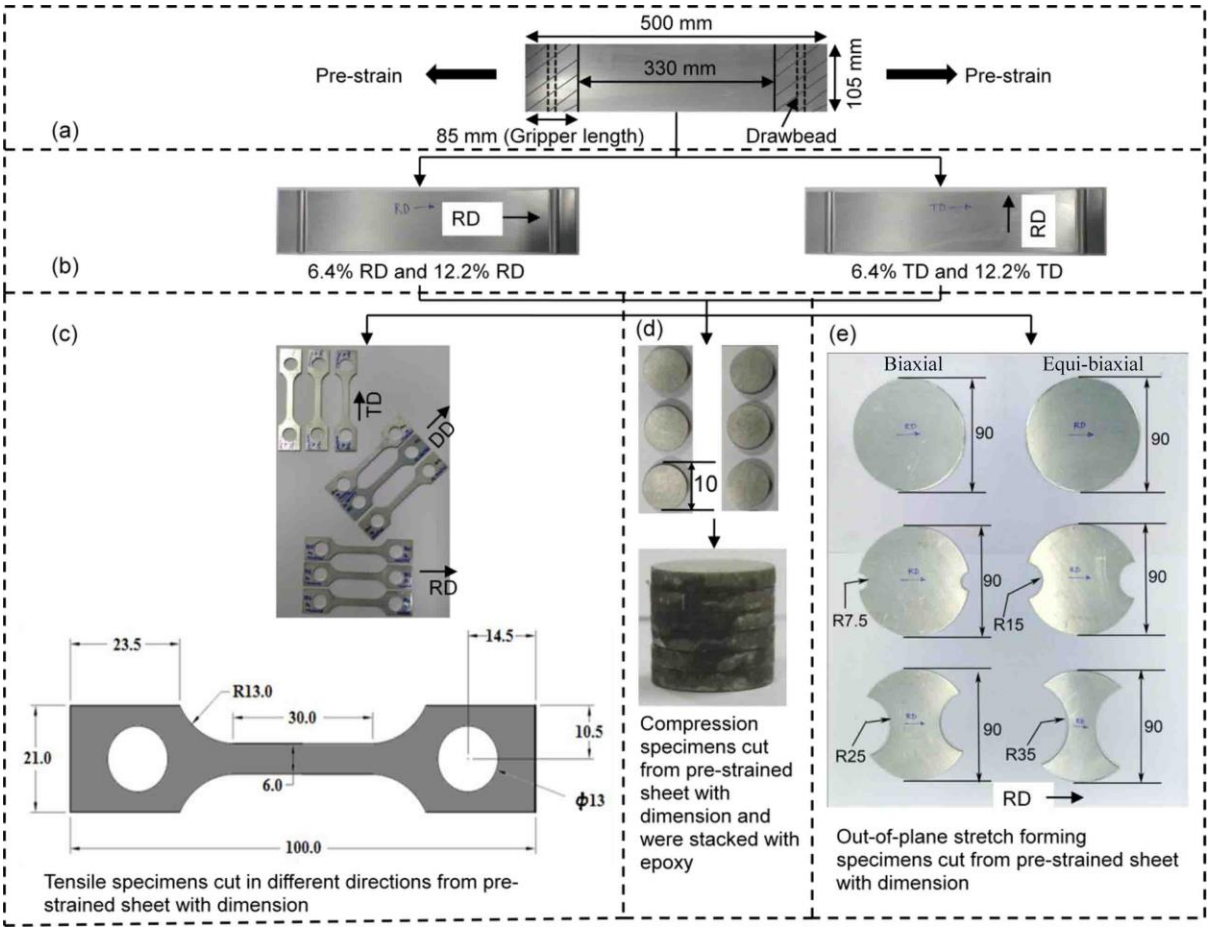

Fig. 2 Detailed process sequences consisting of pre-straining, tensile test, stack compression tests, limiting dome height tests adopted in the present study (all dimensions are in mm)

2.3 Stack compression tests

Previously, researchers had carried out stack compression tests of aluminum-killed steel, aluminum alloy 3003-O, copper-110 and brass 260 (70% copper and 30% zinc) [33]; and magnesium alloy AZ31B-O [34] to evaluate the equi-biaxial flow stress in tensile state. In the present work, circular discs of 10 mm diameter were cut from as-received and pre-strained sheet and six such discs were stacked together to form a solid cylinder as shown in Fig. 2(d).The stacking was done using epoxy adhesive in order to avoid buckling during the compression test. The strength of the adhesive used was approximately 27.3 MPa and it was applied uniformly on the sheet surfaces after roughening using an emery paper. The both ends of the stacked cylinder were lubricated using teflon tape to reduce the frictional force at the contacting surfaces with both the compression platens. The compression testing was performed at a cross-head speed of 2 mm/min using a 50 kN compression machine. The true stress true strain responses of the as

received and pre-strained materials were evaluated and these were considered as the equivalent of biaxial flow curves.

2.4 Limiting dome height tests

The out-of-plane stretch forming set-up consisting of hemispherical punch of ϕ50 mm, upper die and lower die, were mounted in the double action hydraulic press of 100 ton as shown in Fig. 3. The sheet metals were clamped between the upper and lower dies by applying a blank

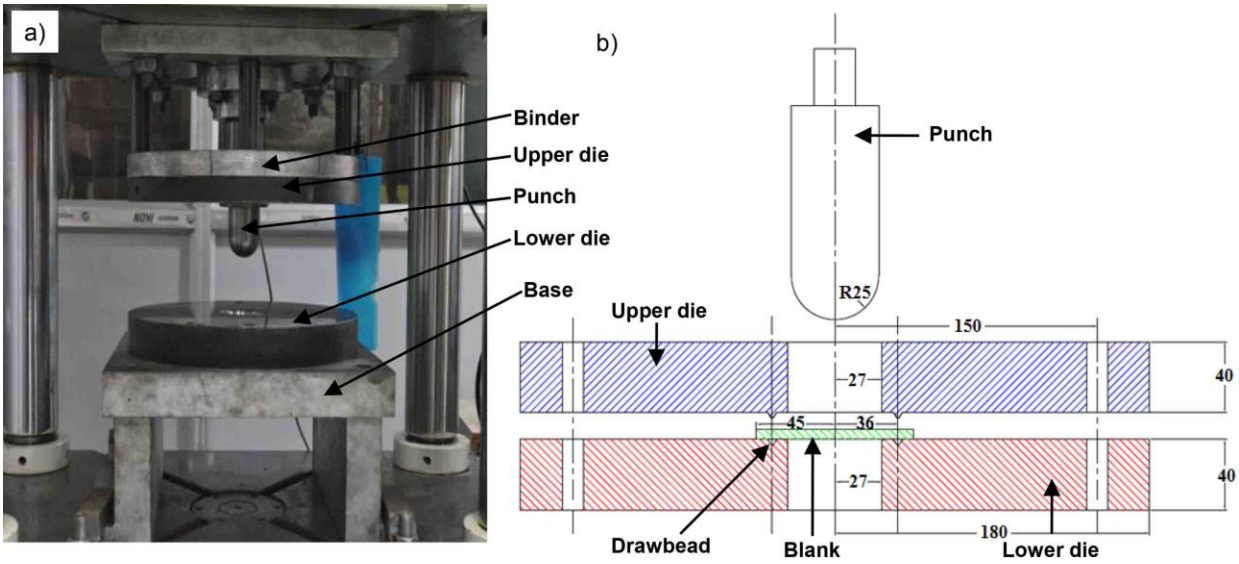

Fig. 3 Out-of-plane stretch forming set-up used to evaluate the LDH and ε-FLDs: (a) the tools mounted in the actual set-up and (b) schematic of tools consisting of punch and dies (all dimensions are in mm)

holding force of 7.7 ton, and the punch was moved down at a speed of 20 mm/min to completely stretch formed the material exposed over the die cavity. A circular drawbead was designed on the dies at a radius of 36 mm, which completely restricted the flange material to flow into the die cavity. The experiments were stopped when a visible neck or initiation of fracture was observed through a mirror placed in the gap below the base of the LDH setup. The height of the dome till the onset of necking was referred as limiting dome height (LDH). Also, a pattern of circular grids of ϕ2.5 mm was applied on the surface of the sheet metals by electrochemical etching method before stretch forming operation. The major and minor true strains were measured from the deformed elliptical grid by imaging software integrated with optical microscope. The experiments were carried out using blanks of five different geometries and application of lubrication as shown in Fig. 2(e), and six different strain paths were induced entirely covering from tension-tension to tension-compression modes during LDH tests by controlling the lateral

material flow during deformation. A close to equi-biaxial tensile deformation mode was achieved using a thin poly-ethylene sheet with lubricating oil between the hemispherical punch and blank. The final deformed domes obtained after the stretch forming operation of as received and four different pre-strained materials are shown in Fig. 4. The major and minor surface strains of safe, necked and failed regions were evaluated to plot the ε-FLDs, and the LDHs were measured using a height gauge.

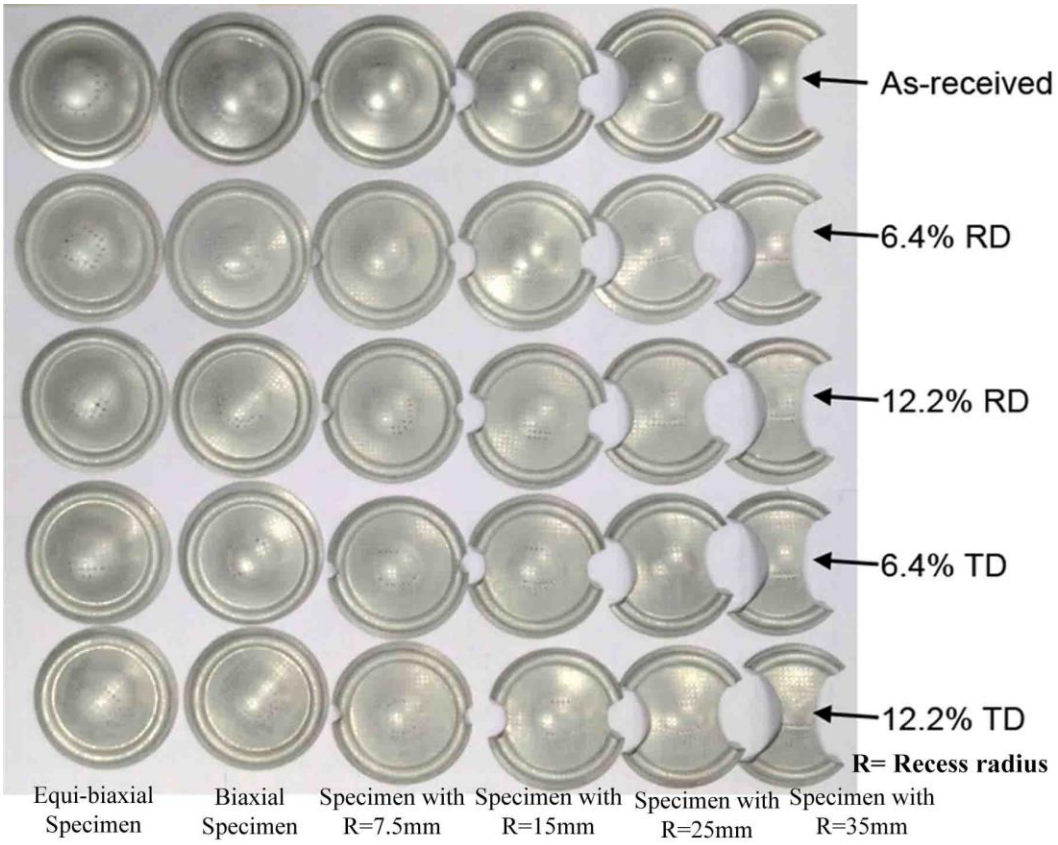

Fig. 4 All the deformed specimens obtained after stretch forming operations of as received and pre-strained materials

3 Development of stress based forming limit diagram

3.1 Background of Yld96 anisotropy plasticity theory

In the present work, the Yld96 anisotropy plasticity theory [35] was considered as it was one of the most accurate yield functions for aluminum alloy sheets incorporating both yield strength and *r*-value directionalities. There were other different advanced yield criteria such as Yld2000, Yld2004, Yld2011, BBC2003, BBC2005 and BBC2008 to consider the deformation behavior of anisotropy sheet metals [36]. However, these models required more number of experiments to

characterize the strength and *r*-value directionalities. The Yld96 yield function was expressed with respect to flow strength of material, $\bar{\sigma}$ as per Eq. (2).

$$\Phi = \alpha_1 \left|S_2 - S_3\right|^a + \alpha_2 \left|S_3 - S_1\right|^a + \alpha_3 \left|S_1 - S_2\right|^a = 2\bar{\sigma}^a \tag{2}$$

Where, the higher order exponent, a = 8 for aluminum being a face centered cubic structure (FCC) material, and S_1, S_2 and S_3 are the principal values of the stress tensor S_{ij}. The isotropic plasticity equivalent (IPE) stress was related to stress tensor as per Eq. (3):

$$\mathbf{S = L\sigma} \tag{3}$$

Where, **L** is connected with anisotropic coefficients c_k (k=1-6). In plane stress condition ($\sigma_z = \sigma_{yz} = \sigma_{zx} = 0$), the Eq. (3) reduced to Eq. (4) as shown below.

$$S_{ij} = \begin{bmatrix} S_x \\ S_y \\ S_z \\ S_{xy} \end{bmatrix} = \begin{bmatrix} \frac{(c_2 + c_3)}{3} & \frac{-c_3}{3} & \frac{-c_2}{3} & 0 \\ \frac{-c_3}{3} & \frac{(c_3 + c_1)}{3} & \frac{-c_1}{3} & 0 \\ \frac{-c_2}{3} & \frac{-c_1}{3} & \frac{(c_1 + c_2)}{3} & 0 \\ 0 & 0 & 0 & c_6 \end{bmatrix} \begin{bmatrix} \sigma_x \\ \sigma_y \\ 0 \\ \sigma_{xy} \end{bmatrix} \tag{4}$$

Here, principal stress values of S_{ij}, can be found by applying Mohr's circle as follows:

$$S_{1,2} = \frac{S_x + S_y}{2} \pm \sqrt{\left(\frac{S_x - S_y}{2}\right)^2 + S_{xy}^2} \tag{5}$$

and $S_3 = -\left(S_1 + S_2\right)$. Further, the anisotropic coefficients α_i of Eq. (2) are defined as:

$$\begin{aligned} \alpha_1 &= \alpha_x \cos^2\beta + \alpha_y \sin^2\beta \\ \alpha_2 &= \alpha_x \sin^2\beta + \alpha_y \cos^2\beta \\ \alpha_3 &= \alpha_{z0} \cos^2 2\beta + \alpha_{z1} \sin^2 2\beta \end{aligned} \tag{6}$$

Where,

$$2\beta = \tan^{-1}\left(\frac{2S_{xy}}{S_x - S_y}\right) \tag{7}$$

3.2 Estimation of anisotropy coefficients and stress ratios for σ-FLD

In the Yld96 anisotropy plasticity theory, the yield behavior of aluminum alloy can be modeled by calculating anisotropic coefficients such as, c_1, c_2, c_3, c_6, α_x, α_y, and α_{z1}. The coefficient, α_{z0} was assumed to be 1.0 as suggested by previous researchers [35, 37]. The above seven coefficients were calculated using seven test results such as: three uni-axial yield strength along the RD (σ_0), DD (σ_{45}) and TD (σ_{90}), balanced biaxial yield strength (σ_b), and three Lankford anisotropic parameter along the RD (r_0), DD (r_{45}), and TD (r_{90}). In the present work, all the seven results such as σ_0, σ_{45}, σ_{90}, σ_b, r_0, r_{45} and r_{90} were evaluated experimentally and seven equations were developed using the testing condition.

For uni-axial tension in the RD, the principal IPE stresses become:

$$S_1 = \frac{(c_2 + c_3)}{3}\sigma_0$$

$$S_2 = -\frac{c_3}{3}\sigma_0 \tag{8}$$

$$S_3 = -\frac{c_2}{3}\sigma_0$$

The yield function in Eq. (2) can then be written as:

$$\alpha_x |c_2 - c_3|^a + \alpha_y |2c_2 + c_3|^a + \alpha_{z0} |c_2 + 2c_3|^a - 2\left(\frac{3\bar{\sigma}}{\sigma_0}\right)^a = 0 \tag{9}$$

Similarly, the equations for uni-axial tension in the DD and the TD and the balanced biaxial tension can be expressed as Eq. (10), Eq. (11) and Eq. (12) respectively:

$$\alpha_x |2c_1 + c_3|^a + \alpha_y |c_3 - c_1|^a + \alpha_{z0} |2c_3 + c_1|^a - 2\left(\frac{3\bar{\sigma}}{\sigma_{90}}\right)^a = 0 \tag{10}$$

$$\alpha_1 \left| (c_1 + c_2) - \sqrt{\left(\frac{c_2 - c_1}{3}\right)^2 + (2c_6)^2} \right|^a + \alpha_2 \left| (c_1 + c_2) + \sqrt{\left(\frac{c_2 - c_1}{3}\right)^2 + (2c_6)^2} \right|^a$$

$$+\alpha_3 \left| \sqrt{\left(\frac{c_2 - c_1}{3}\right)^2 + (2c_6)^2} \right|^a - 2\left(\frac{2\bar{\sigma}}{\sigma_{45}}\right)^a = 0 \tag{11}$$

where α_1, α_2 and α_3 are as defined by Eq. (6).

$$\alpha_x\left|2c_1+c_2\right|^a+\alpha_y\left|2c_2+c_1\right|^a+\alpha_{z0}\left|c_2-c_1\right|^a-2\left(\frac{3\bar{\sigma}}{\sigma_b}\right)^a=0 \tag{12}$$

Using normality rule, $d\varepsilon_{ij}=d\lambda\frac{\partial\Phi}{\partial\sigma_{ij}}$ (where $d\lambda$ is a positive instantaneous constant) in the definition of Lankford anisotropy plasticity theory in Eq. (1), the r_θ can be expressed as Eq. (13).

$$r_\theta=\frac{\frac{\partial\Phi}{\partial\sigma_{90+\theta}}}{\frac{\partial\Phi}{\partial\sigma_{zz}}}=-\frac{\frac{\partial\Phi}{\partial\sigma_{90+\theta}}}{\left(\frac{\partial\Phi}{\partial\sigma_{90+\theta}}+\frac{\partial\Phi}{\partial\sigma_\theta}\right)}=-\frac{\frac{\partial\Phi}{\partial\sigma_x}\sin^2\theta+\frac{\partial\Phi}{\partial\sigma_y}\cos^2\theta-2\frac{\partial\Phi}{\partial\sigma_{xy}}\cos\theta\sin\theta}{\left(\frac{\partial\Phi}{\partial\sigma_x}+\frac{\partial\Phi}{\partial\sigma_y}\right)} \tag{13}$$

Three equations were generated for r_0, r_{45} and r_{90} putting θ = 0°, 45° and 90°, and the yield function Φ in Eq. (2). All seven equations consisting of four stress equations (Eq. (9) to Eq. (12)) and three *r*-value equations (derived from Eq. (13)) were solved for the values of the anisotropy coefficients c_1, c_2, c_3, c_6, α_x, α_y, and α_{z1} using Newton–Raphson non-linear solver available in MATLAB. Similar procedure was also adopted by previous researchers [35, 37].

Applying normality rule, in Eq. (2), the strain ratio (ratio of minor strain to major strain) can be obtained as in the form of stress ratio (ratio of minor stress to major stress) as shown in Eq. (14).

$$\rho=\frac{Q\alpha_1\left|P+Q\alpha\right|^{(a-1)}+S\alpha_2\left|R+S\alpha\right|^{(a-1)}+U\left|T+U\alpha\right|^{(a-1)}}{P\alpha_1\left|P+Q\alpha\right|^{(a-1)}+R\alpha_2\left|R+S\alpha\right|^{(a-1)}+T\left|T+U\alpha\right|^{(a-1)}} \tag{14}$$

Where, $\rho=\frac{\varepsilon_2}{\varepsilon_1}$ = strain ratio, $\alpha=\frac{\sigma_2}{\sigma_1}$ = stress ratio, $P=\left(c_2-c_3\right)/3$, $Q=\left(2c_1+c_3\right)/3$, $R=-\left(2c_2+c_3\right)/3$, $S=\left(c_3-c_1\right)/3$, $T=\left(c_2+2c_3\right)/3$ and $U=-\left(2c_3+c_1\right)/3$.

Another parameter ξ is defined as the ratio of the effective stress and major stress, and it can be expressed in the following form as shown in Eq. (15).

$$\xi=\frac{\bar{\sigma}}{\sigma_1}=\left[\tfrac{1}{2}\cdot\left\{\alpha_1\left|P+Q\alpha\right|^a+\alpha_2\left|R+S\alpha\right|^a+\left|T+U\alpha\right|^a\right\}\right]^{1/a} \tag{15}$$

Imposing the plane stress condition in the definition of plastic work, the effective strain can be expressed as Eq. (16).

$$\bar{\varepsilon} = \left(\varepsilon_1\left(1+\rho\alpha\right)\right)\Big/\xi \tag{16}$$

The detailed procedure, discussed by Basak et al [31], was followed here to develop σ-FLD from experimental ε-FLD of AA5754-O. The major (ε_1) and minor (ε_2) strain (true strain) values were noted from the experimentally evaluated ε-FLD. From the knowledge of strain ratio ρ, both the stress ratio α and the parameter ξ were estimated using Eq. (14) and (15) respectively. Using Eq. (16), the effective strain $\bar{\varepsilon}$ was calculated and moreover the effective stress $\bar{\sigma}$ was estimated using the Hollomon hardening law. The major stress value σ_1 was calculated using the Eq. (15) and the minor stress value σ_2 was calculated using the stress ratio α. These estimated limiting stresses σ_1 (major true stress) and σ_2 (minor true stress) were plotted to get σ-FLD corresponding to the ε-FLD to predict failure in the numerical simulation.

4 Numerical simulation

In this work, two different finite element (FE) models were developed and subsequently solved using commercially available LS-DYNA software of version 971. These were: (i) at first, the uni-axial pre-straining operation of as-received sheet along RD and TD with 6.4% and 12.2% pre-strain and further (ii) the out-of-plane stretch forming operation of the pre-strained sheet along with as-received sheet. The FE model with the typical process sequence consisting of pre-straining, trimming and out-of-plane stretch forming is depicted in Fig. 5. In the out-of-plane stretch forming process, all the tooling surfaces such as the die, punch and blank holder (or binder) were modeled as rigid bodies, and these were meshed with shell elements taking proper care of the warpage angle. The quarter symmetry model was developed to reduce the computational time. The deformable blank was modeled as four-nodded quadrilaterals Belytschko–Tsay elements (considering five through thickness integration points) with adaptive remeshing scheme, and the Yld96 yield material model was assigned as discussed in section 3.1. The trimmed pre-strained blank was kept over the stationary die with assigned blank holding force, and the punch was assigned to move along Z-axis. The coulomb's sliding friction model with coefficient of friction of 0.15 was assigned between the punch and blank in dry condition and 0.05 in case of lubricated condition. The σ-FLD estimated from experimentally evaluated ε-FLD of as-received material was considered as the damage model to predict the onset of failure as soon as the stress state during deformation touched the limiting stress.

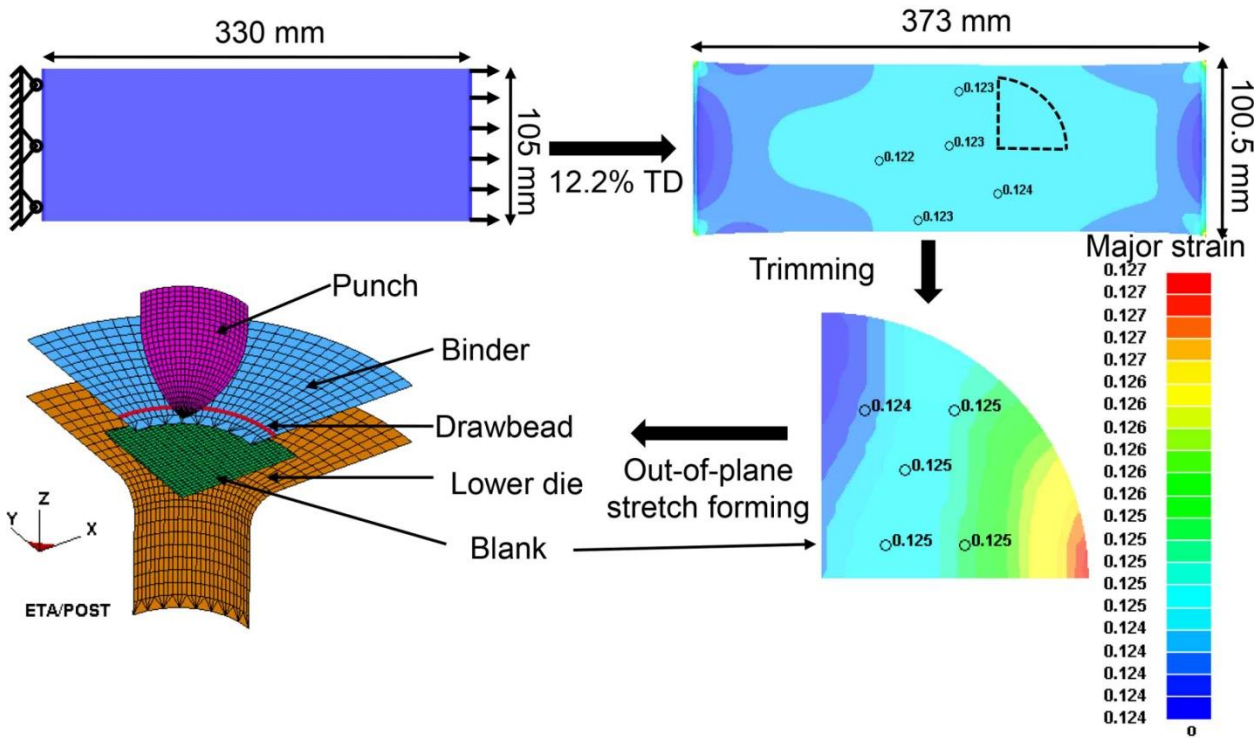

Fig. 5 FE modeling of the out-of-plane stretch forming of uni-axial pre-strained material

5 Results and discussion

5.1 Effect of pre-strain on tensile properties

The average tensile properties such as yield strength (YS), ultimate tensile strength (UTS), total elongation, Lankford anisotropy parameters (r_0, r_{45} and r_{90}), normal anisotropy parameter ($\bar{r}$) and planar anisotropy parameter (Δr) of as-received and four different pre-strained materials evaluated from uni-axial tensile test (designated as UT in Fig. 6 and 7) are compared in Table 2. It was observed that the yield strength of the pre-strained materials increased with the decrease in the ductility (in terms of elongation) due to strain hardening. Also, it was observed that the uni-axial pre-straining (designated as UP in Fig. 6 and 7) along TD resulted higher yield strength and ultimate tensile strength in comparison with pre-straining along RD. However, the difference in strength of the material was very negligible on applications of equal amount of pre-strain along RD and TD. There was change in the r_0, r_{45}, r_{90}, $\bar{r}$ and Δr with the amount and direction of pre-straining, but no particular trend was observed. The 1.54 mm thick as-received sheet decreased to a thickness of 1.49 mm and 1.44 mm on applications of 6.4% and 12.2% pre-strain. The comparison of true stress-strain responses of as-received and different pre-strained material along different directions is shown in Fig. 6(a) and (b). It can be observed that all data make a

band matching reasonably close to the fitted Hollomon strain hardening law along RD of as-received material. It may be concluded that the pre-straining did not alter significantly the flow strength of the material. The Hollomon equation correlating the true stress-true strain response of all these materials tested along rolling direction are shown in Table 3.

Table 2 Tensile properties of as-received and pre-strained materials during uni-axial tensile test

Pre-straining condition	Yield strength (MPa)	Ultimate tensile strength (MPa)	% Total elongation	Anisotropic properties					Thickness of sheet after pre-straining (mm)
				r_0	r_{45}	r_{90}	$\bar{r}$ *	Δr **	
As-received	101.88	225.86	35.63	0.861	0.523	0.756	0.666	0.286	1.54
6.4% RD	169.58	236.39	19.99	0.685	0.463	0.632	0.561	0.196	1.49
6.4% TD	173.11	240.95	16.52	0.753	0.476	0.676	0.595	0.238	1.49
12.2% RD	211.44	253.24	13.34	0.648	0.389	0.631	0.514	0.250	1.44
12.2% TD	215.11	256.22	11.85	0.649	0.438	0.608	0.533	0.190	1.44

* $\bar{r} = (r_0+2r_{45}+r_{90})/4$

** $\Delta r = (r_0-2r_{45}+r_{90})/2$

It can be found that the strength coefficient (*K*-value) and the strain hardening exponent (*n*-value) changed in comparison to that of as-received material. The biaxial true stress-true strain responses of the as-received and different pre-strained materials were also evaluated from the stack-compression test (designated as SC in Fig. 7) and these results were compared with the uni-axial tensile tests results tested along RD in Fig. 7.

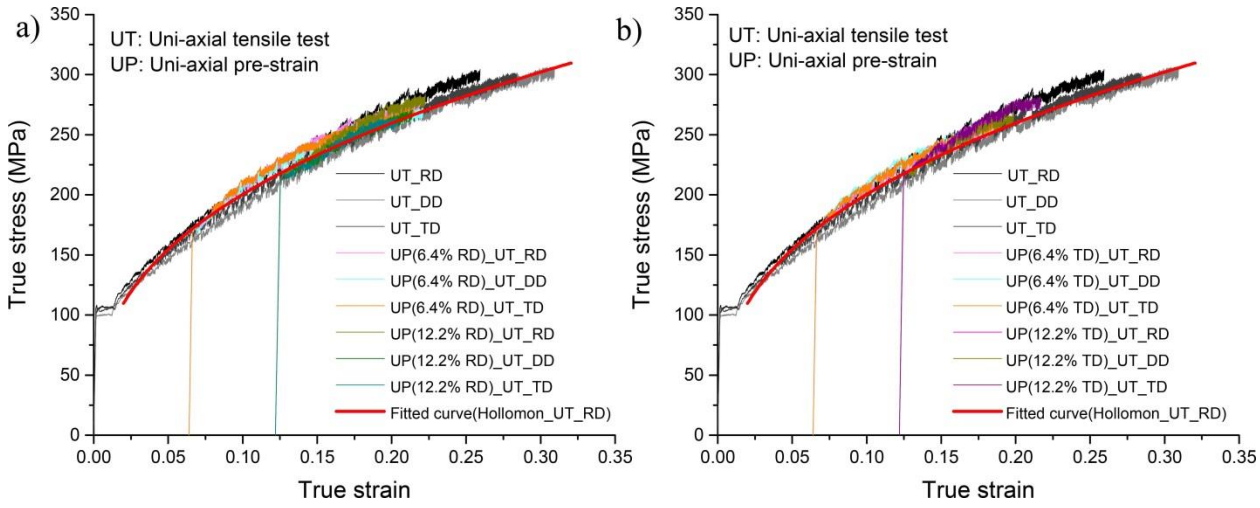

Fig. 6 True stress-strain response during uni-axial tensile test of as-received and pre-strained materials along (a) rolling direction and (b) along transverse to rolling direction

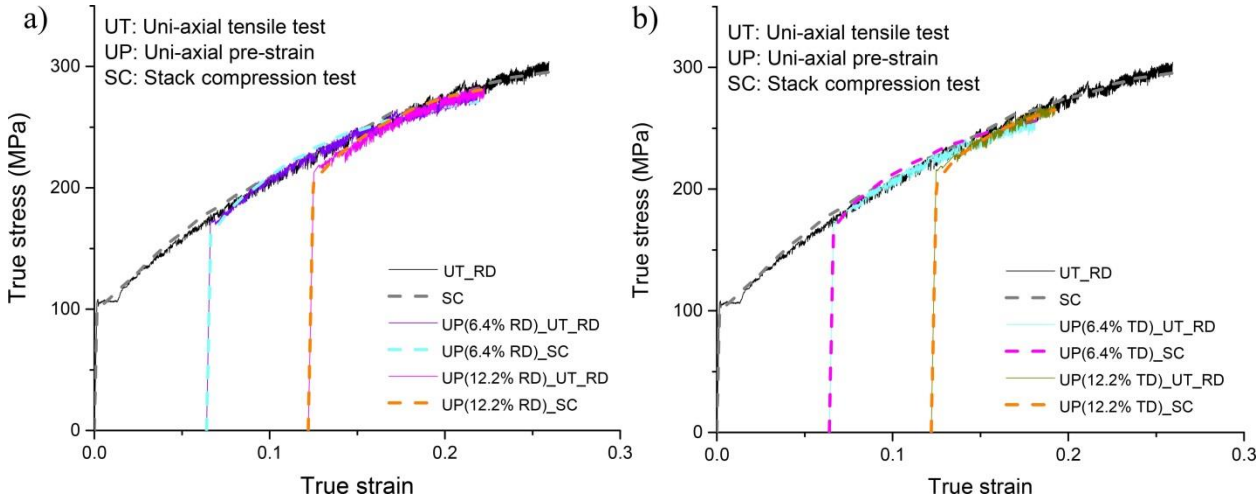

Fig. 7 Comparison of true stress-strain response during uni-axial tensile and stack compression test of as-received and pre-strained materials along (a) rolling direction and (b) along transverse to rolling direction

Table 3 Material constants of as-received and pre-strained materials along RD during uni-axial tensile test

Pre-straining condition	Hollomon equation $\bar{\sigma} = K\bar{\varepsilon}^{n}$	R^{2*}
As-received	$\bar{\sigma} = 490.29\bar{\varepsilon}^{0.370}$	0.991
6.4% RD	$\bar{\sigma} = 549.20\bar{\varepsilon}^{0.416}$	0.983
6.4% TD	$\bar{\sigma} = 520.00\bar{\varepsilon}^{0.358}$	0.981
12.2% RD	$\bar{\sigma} = 661.70\bar{\varepsilon}^{0.529}$	0.960
12.2% TD	$\bar{\sigma} = 684.60\bar{\varepsilon}^{0.530}$	0.963

* R^2 is termed as coefficient of determination

5.2 Yield loci of as received and pre-strained materials using Yld96 model

From all the stress-strain responses discussed in the section 5.1, the yield strengths of as-received and pre-strained AA5754-O alloy were evaluated in different direction during tensile tests and stack compression tests. These results in conjunctions with the evaluated Lankford anisotropy parameters r_0, r_{45} and r_{90} were used to estimate the different Yld96 anisotropy coefficients such as c_1, c_2, c_3, c_6, α_x, α_y, and α_{z1} as discussed in section 3.2. All these estimated anisotropy coefficients for the as-received and the four different pre-strained materials are summarized in Table 4. The yield loci of the as-received and four different pre-strained materials were plotted using their respective anisotropy coefficients as shown in Fig. 8(a), and the experimental data were shown for comparisons. From the experimental data it was observed that yield loci were expanding in size with a negligible distortion in shape (Fig.8.a). Hence isotropic hardening law (Hollomon hardening law) was indulged into the formulation with the anisotropic yield criterion (Yld-96) to predict the expansion of the yield loci of the pre-strained materials depending on the effective plastic strain. It was found that the predicted yield loci matched reasonably with the experimental data of pre-strained materials. Further, the entire experimental yield data points matched very well with the Yld96 yield locus when plotted in normalized stress space as shown in Fig. 8(b). The distortion in the yield loci of the pre-strained materials was negligible compared to that of as received material, and the Hollomon isotropic hardening model with Yld96 plasticity model of as-received material could able predict the yield behavior of different pre-strained material reasonably well.

Table 4 Evaluated anisotropic coefficients of as-received and pre-strained materials

Pre-straining condition	c_1	c_2	c_3	c_6	α_x	α_y	α_{zl}
As-received	0.9879	1.0080	0.9827	1.1624	1.304	1.072	1.212
6.4% RD	0.9216	0.9333	0.9883	1.0968	1.997	1.809	1.355
6.4% TD	0.9129	0.9831	0.9784	1.1542	1.843	1.334	1.069
12.2% RD	0.9027	0.8915	0.9994	1.0678	2.284	2.297	1.421
12.2% TD	0.9235	0.9805	0.9648	1.1223	1.881	1.486	1.394

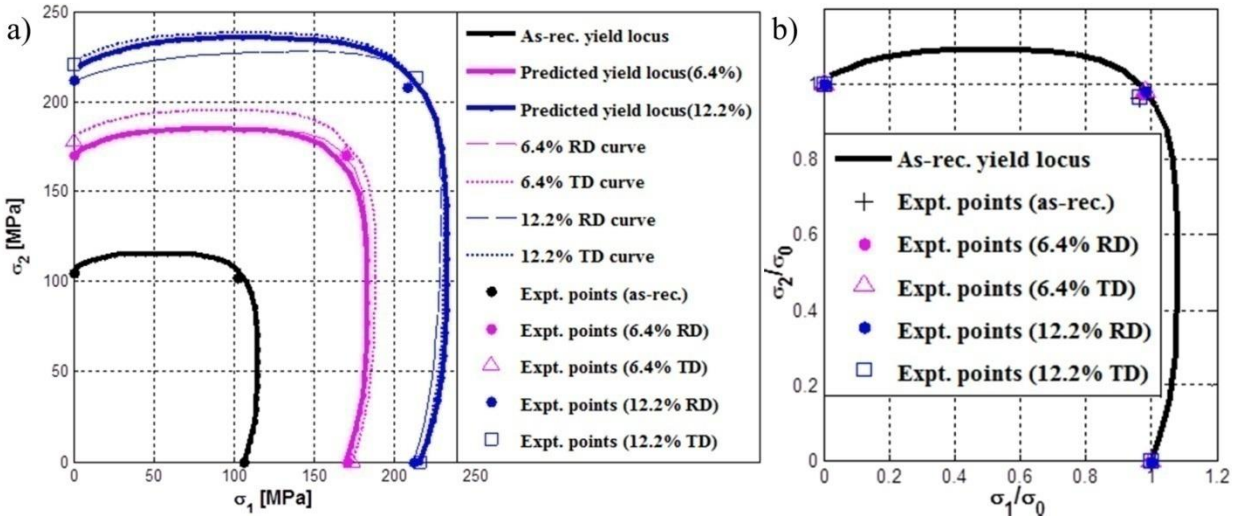

Fig. 8 Validation of Yld96 plasticity theory: (a) expansion of yield locus for different pre-strained conditions and (b) yield locus in normalized stress space

5.3 Effect of pre-strain on forming limit diagram

The major and minor strain data of failed, necked and safe ellipses on the surface of all the deformed specimens were plotted, and the ε-FLD was constructed separating the safe zone. It can be found that the strain path changed over a wide range from ρ =0.98 to -0.47 by selecting five different specimen geometries and application of lubrication. The limiting strain in the ε-FLD was found to be the lowest (ε_1=0.206 and ε_2=0 for as-received material) when the sheet material was deformed under a strain path of $\rho = 0$ (i.e. in plane strain deformation mode). The major and minor true strain data ($\varepsilon_1, \varepsilon_2$) in the ε-FLD were converted to stress space using the Yld96 plasticity theory as discussed in section 3.2 to estimate the σ-FLD. The estimated σ-FLD of the AA5754-O aluminum alloy with the corresponding stress paths of 12.2% TD pre-strained conditions is shown in Fig. 9(b). It was observed from Fig. 9 that nearly uni-axial deformation

path (marked by OA in strain and stress space) was induced in the specimen. In the second stage, the deformation paths of two different geometries were shown. The deformation path AX and AX' were representing for biaxial specimen and a specimen with recess radius 35 mm respectively.

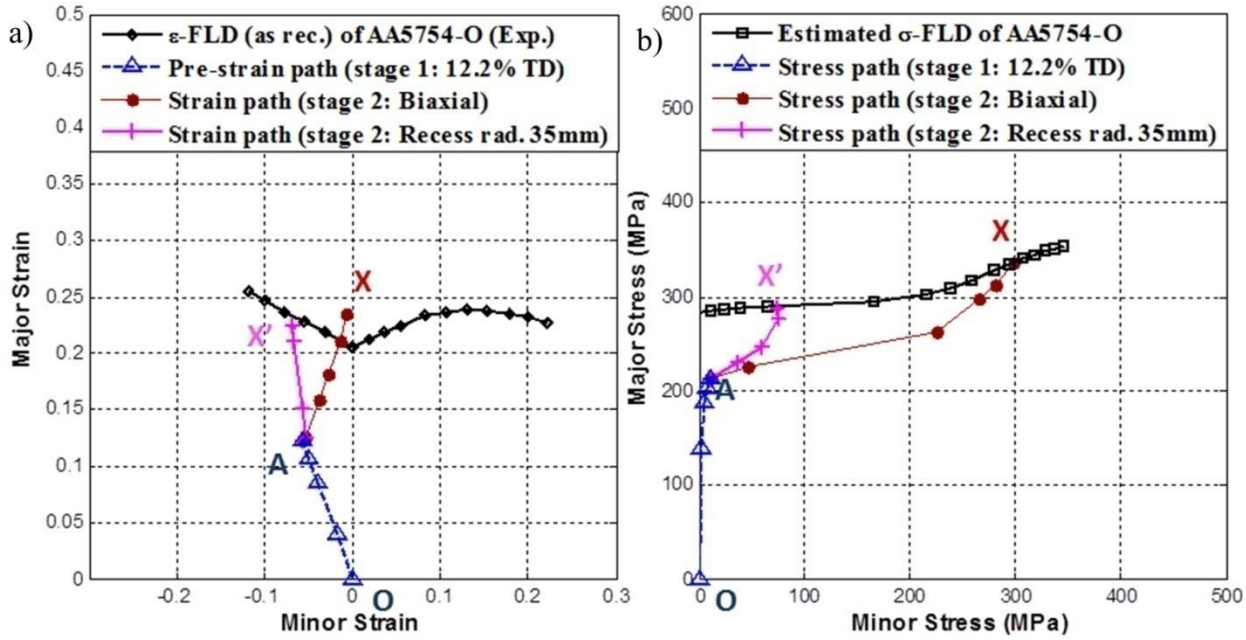

Fig. 9 (a) Experimental strain based and (b) estimated stress based forming limit diagram of as-received sheet metal

During LDH test of pre-strained material, it was observed that the experimental ε-FLD shifted from its original position. This phenomenon was termed as 'dynamic shift of the limiting strains'. In this study, the σ-FLD evaluated from experimental ε-FLD of as-received material was further considered for evaluating the 'dynamic shift of the limiting strains' of the pre-strained materials. This process is known as the 'decoupling of σ-FLD'. Here, the σ-FLD is decoupled to obtain ε-FLDs of different pre-strained material. This is a novel attempt of theoretical prediction of the dynamically shifted pre-strained ε-FLD. Accordingly, σ-FLD was decoupled into strain space for 6.4% and 12.2% uni-axial pre-strain along RD and TD. Detailed decoupling procedure was adopted from the previous works [31]. However for better understanding to the readers, the decoupling formulation was discussed below in five simple steps.

a) To evaluate the limiting strains for a definite pre-strain, the major (σ_1) and minor (σ_2) true stress values were noted from the σ-FLD of AA5754-O as shown in Fig. 9(b). After

calculating the stress ratio α, different parameters like ρ and ξ were evaluated by using Eq. (14) and (15), respectively.

b) Effective stress ($\bar{\sigma}$) was calculated from σ_1 and ξ as per Eq. (15). Total effective strains ($\bar{\varepsilon}$) after forming in both the stages (uni-axial pre-straining and LDH testing) were obtained from the Hollomon hardening law.

c) Now, the effective strain ($\bar{\varepsilon}_P$) during pre-straining was evaluated from the amount of pre-strain value (ε_{1P}, ε_{2P}), as per Eq. (16). Finally, the effective strain in the final stage ($\Delta\varepsilon_f$) was calculated using Eq. (17).

$$\Delta\varepsilon_f = f\left\{\bar{\varepsilon}\left(\sigma_1,\sigma_2\right) - \bar{\varepsilon}_P\left(\varepsilon_{1P},\varepsilon_{2P}\right)\right\} \quad (17)$$

d) From the definition of plastic work Eq. (16), increment in major and minor strain ($\Delta\varepsilon_1$ and $\Delta\varepsilon_2$) were calculated from ρ_f (strain ratio at stretch forming stage).

e) Using Eq. (18), the major (ε_{1f}), minor (ε_{2f}) strain points of decoupled ε-FLD were calculated and plotted in Fig. 10 for various uni-axial pre-strain conditions.

$$\varepsilon_{1f} = \varepsilon_{1P} + \Delta\varepsilon_1 \text{ and } \varepsilon_{2f} = \varepsilon_{2P} + \Delta\varepsilon_2 \quad (18)$$

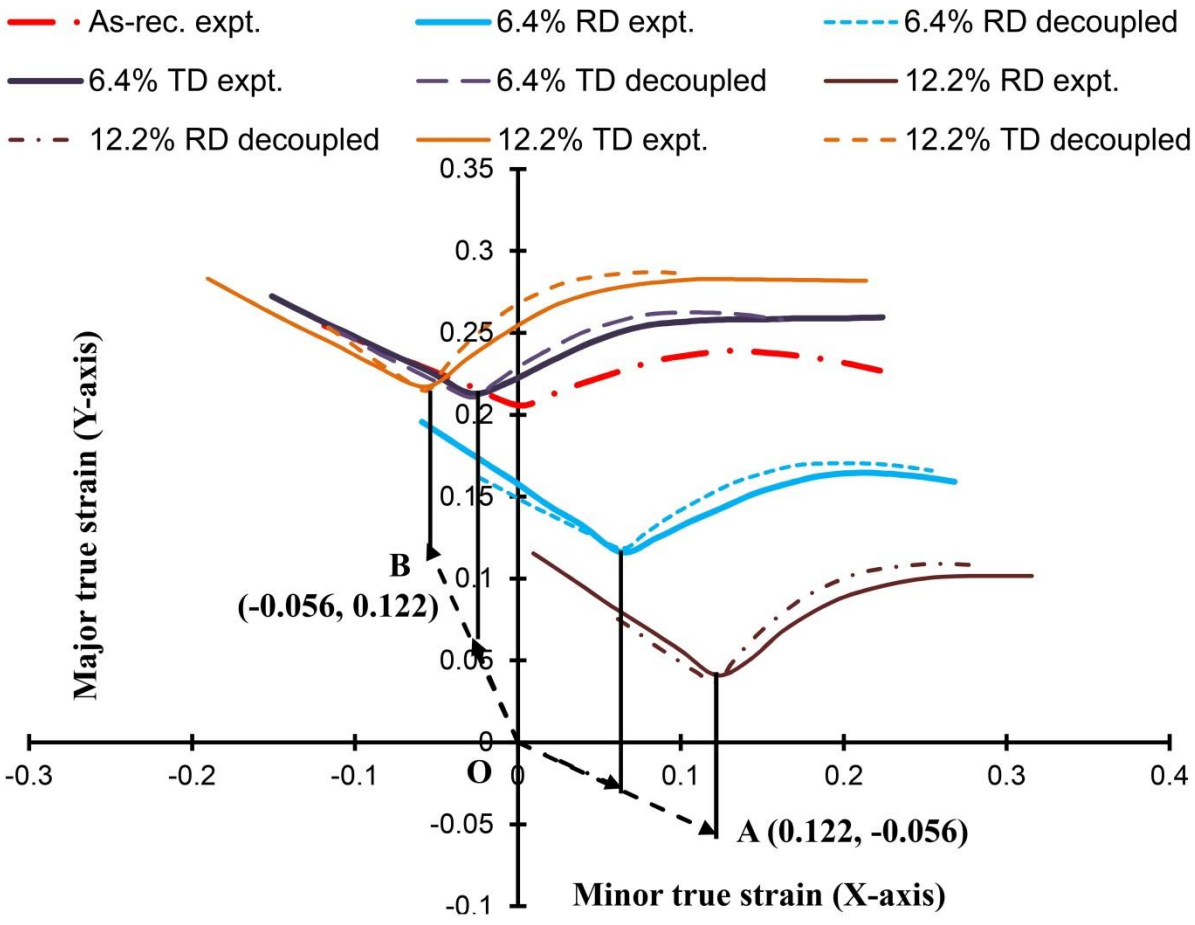

Fig. 10 Comparison of experimental and decoupled ε-FLDs for different pre-straining conditions

All the experimentally evaluated ε-FLDs of different pre-strain materials are compared with the decoupled limiting strains estimated from the σ-FLD as shown in Fig. 10. It was observed that the ε-FLDs shifted significantly depending on the amount and the orientation of pre-strain with respect to RD. Here, rolling direction (RD) and transverse direction (TD) true strains were plotted along X and Y axis respectively. During pre-straining in RD, the circles were elongated along X axis, whereas compressed along Y axis. Therefore the minor true strain was positive and major true strain was negative (shown by OA line in Fig.10). On contrary during TD pre-straining, the circles were compressed along X axis and elongated along Y axis. Hence, minor true strain was negative and major true strain was positive (shown by OB line in Fig.10). This was the reason behind the massive shifting of the ε-FLD curves depending on the RD and TD pre-strain. If the RD pre-strained ε-FLD curve was translated in such a way that the line OA got superimposed with OB, then it could be observed that there was a minor difference in limiting strains depending on the direction of pre-strain. Again it was observed in Fig 6, that ductility loss (in terms of % elongation) was less in case of 6.4% pre-strained sheet compare to 12.2% pre-strained sheet. Hence the amount of shifting of the ε-FLD was also different depending on the level of pre-strain. It was observed in Fig 10 that the pre-strain along TD shifted ε-FLD towards the left side with increase in the forming limit strains. However, the limiting strains of the material decreased with right side shifting of ε-FLD for pre-strained material along RD. The error (Root Mean Square Error, RMSE) of true strain values between experimental and decoupled ε-FLDs for each case of pre-strained conditions were evaluated by using Eq. (19).

$$\mathrm{RMSE} = \sqrt{\frac{\sum (\varepsilon_{1\mathrm{expt.}} - \varepsilon_{1\mathrm{decoupled}})^2}{N}} \tag{19}$$

Where $\varepsilon_{1\mathrm{expt.}}$ = major true strain in experimental ε-FLD, $\varepsilon_{1\mathrm{decoupled}}$ = major true strain in decoupled ε-FLD and N= No. of strain data point. These errors are shown in Table 5 and it can be observed that the error is higher in case of 12.2% pre-strain condition compared to 6.4% pre-strain. However, all the errors are very negligible and the σ-FLD can be used as forming limit for as-received and all the pre-strained materials.

Table 5 Root mean square error (RMSE) of strain values between experimental and decoupled ε-FLDs

Pre-straining condition	RMSE
6.4% RD	0.008076
6.4% TD	0.005092
12.2% RD	0.010763
12.2% TD	0.008781

5.4 Effect of pre-strain on limiting dome height

The average LDH of the as-received and pre-strained materials of AA5754-O are enlisted in Table 6 and the high repeatability of the results are further specified in terms of negligible variation. It can be found that the LDH of the pre-strained materials are lower compared to that of as-received materials. Moreover, the LDH decreased with the increase in pre-strain in the case of all specimen geometries and lubrication conditions. Lower LDH was observed in the case of pre-strained materials along TD compared to that in the pre-strained materials along RD. However the difference in LDH was very negligible instead of significant shift of ε-FLDs depending on the direction of pre-straining. This was because of approximately similar quantity of effective strain induced in the material during the pre-straining irrespective of pre-straining direction. For example 12.2% pre-strain specimen along RD, the major and minor strains induced in the specimen were -0.056 and 0.122 respectively (defined by OA line). Similarly for 12.2% pre-strain along TD, the major and minor strains induced in the specimen were 0.122 and -0.056 respectively (defined by OB line). The effective plastic strain calculated using Eq.16 was 0.122 in case of above two different pre-strained specimens. Consequently, the ductility losses were identical for both the specimens. This can be reconfirmed from the uniaxial tensile test result. From Fig.6, it was observed that the consumed ductility (in terms of % elongation) were equal after 12.2% uniaxial pre-straining in case of both directions. This led to the nearly equal LDH observed for both of the specimen as mentioned earlier in this paragraph.

Table 6 Experimental LDHs after out-of-plane stretch forming operation

Pre-straining condition	LDH (in mm) of different stretch formed specimens					
	Equi-biaxial specimen	Biaxial specimen	Specimen with recess radius 7.5 mm	Specimen with recess radius 15 mm	Specimen with recess radius 25 mm	Specimen with recess radius 35 mm
	Lubricated condition	Dry condition				
As-received	19.03±0.18	16.18±0.23	13.91±0.20	13.55±0.24	13.31±0.16	14.41±0.22
6.4% RD	17.52±0.21	12.86±0.19	12.75±0.15	11.16±0.25	10.98±0.17	10.19±0.18
6.4% TD	17.18±0.19	12.42±0.22	12.52±0.17	10.99±0.18	10.64±0.26	9.98±0.32
12.2% RD	16.28±0.23	12.09±0.17	11.97±0.21	11.09±0.16	10.29±0.20	9.48±0.19
12.2% TD	15.96±0.17	11.83±0.20	11.63±0.19	10.83±0.21	10.03±0.18	9.22±0.24

5.5 Validation of FE prediction

To predict the formability of as-received and pre-strained material, FE simulation of out-of plane stretch forming of few selective cases were carried out. The predicted LDH results were compared with the experimental data as shown in Fig. 11. Predicted stress and strain path for 12.2% TD pre-strained AA5754-O were plotted inside ε-FLD and σ-FLD in Fig. 9. It was observed that, according to σ-FLD (predicted by as-received Yld96 coefficients as discussed later in this sub-section) the failure step for tension-tension and tension-compression specimens were marked by X and X' point respectively in Fig. 9(b). Whereas in ε-FLD, the strain values of corresponding points were not lying on the ε-FLD. The LDH of different points which were lying exact on both of the FLDs were recorded and shown in Fig. 11. It was observed that the LDHs were predicted very well using the estimated σ-FLD and the Yld96 anisotropy plasticity model. Now for estimating σ-FLD from the evaluated Yld96 coefficients, two different methods were adopted in this work. In first method (designated as σ-FLD_M1), the σ-FLDs were estimated using the Yld96 coefficients in as-received conditions (refer Table 4). For second method (designated as σ-FLD_M2), the σ-FLDs were evaluate based on the modified coefficients calculated for each of the pre-strained cases. From the estimated LDH values, it was concluded that modified coefficients yielded better results compare to as received coefficients. But, these differences in prediction by both of the coefficients were ranging from 1-5%. On the

other hand, it requires a considerable effort for determining the modified coefficients for each of the pre-strained cases. Hence, using as-received coefficients for predicting σ-FLD is a better choice to avoid of complexity and save time and effort during computation.

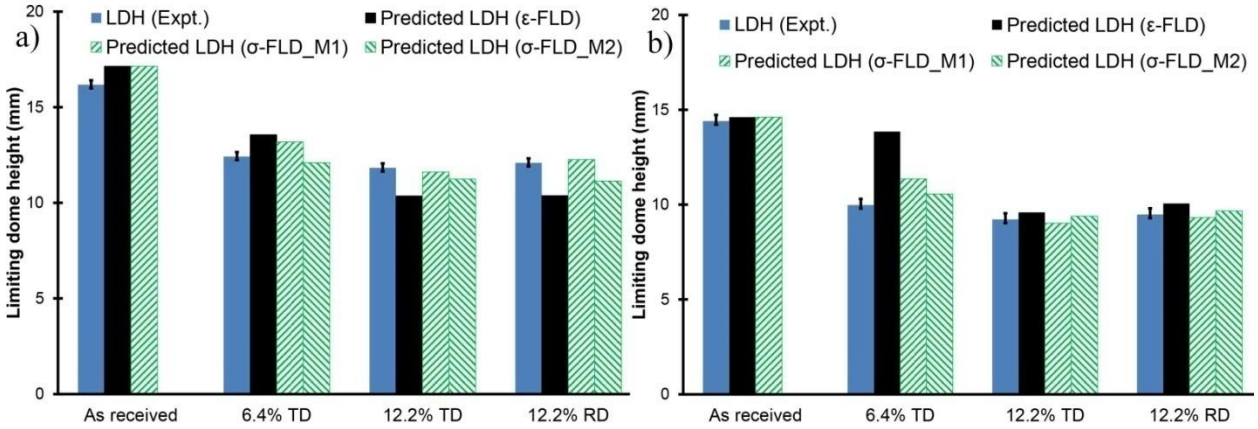

Fig. 11 Comparison of experimental and predicted LDHs for (a) biaxial and (b) recess radius of 35 mm specimens for selected pre-straining conditions

In some of the recent literatures, the researchers showed their concern about the dependency of σ-FLD on the in-plane anisotropy coefficients while estimating σ-FLD from a given ε-FLD [38, 39]. More recently Hariharan et al. [40] used a relatively new approach for predicting σ-FLD based on geometrical interpolation along different strain paths. But in the present work, the mechanical properties of two different pre-strained specimens (viz. pre-strained along RD and TD) were evaluated separately. Further, the validation of FE model in terms of thickness distribution was primary concern in the present work. Hence, the deformed domes of as-received and pre-strained materials were cut along the TD, and the thickness variation was measured at different distances from the pole (dome center or the topmost position of the dome) using a pointed anvil micrometer. The thickness distributions in deformed dome of four different cases were shown in the Fig. 12 to get insight into the effect of amount and direction of pre-strain and the geometry of the specimen. It was observed that the thickness distribution was symmetrical with negligible amount of thinning at the pole. It was due to the cup deformed using the axi-symmetric punch and dies. Also, the punch came in contact with the blank from the start of deformation and the frictional force did not allow the flow of material over the punch surface close to pole. The thinning in the flange was negligible as it was completely locked and was not allowed to flow into the die cavity. The deformation was mostly observed due to the stretching of the material exposed over die cavity with maximum thinning development at certain distance

away from the pole where the deformed cup was starting to be out-of-contact with the punch. The exact location of the maximum thinning was measured in case of as-received and selective pre-strained deformed cups, and the result was shown in Fig. 12. It was observed that the location of failure shifts towards the pole for pre-strained material. Also the LDH observed was less compared to that of as-received specimen. Hence, the area of contact between the punch and blank decreased with the decrease in LDH. Correspondingly, the location of maximum thinning shifted towards the pole in the case of pre-strained materials. Further the maximum thinning location moved very close to pole in case of narrower specimens, and it was approximately 5 mm distance (marked by OC in Fig. 12) in the case of 12.2% TD pre-strained specimens. But for as-received specimen the maximum thinning location was at 16 mm (marked by OA in Fig. 12) from the pole. The FE predicted results were compared with the experimental data points and very close agreement were found. It was observed in Fig.12 that the thickness distribution profiles were comparatively identical for both 12.2% TD and 12.2% RD cases. Hence, the thickness distribution and the maximum thinning location were found not to be influenced much by the uni-axial pre-strain direction.

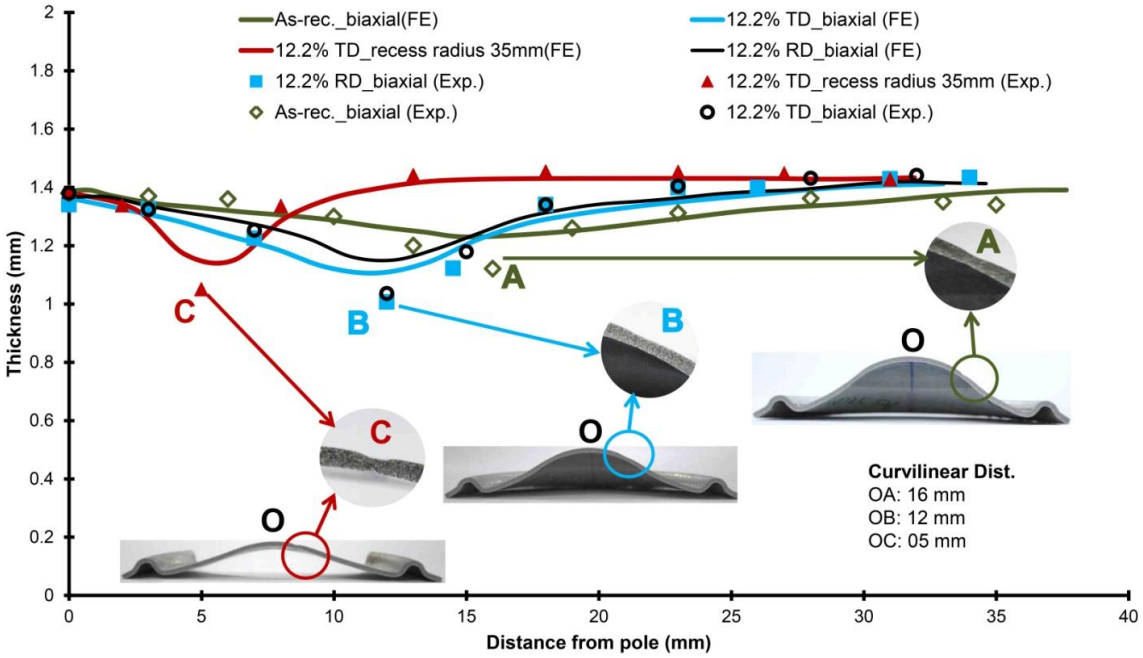

Fig. 12 Comparison of experimental and predicted thickness distribution of stretch formed domes

6 Conclusions

In the present work, the tensile properties, limit dome height and forming limit diagram of pre-strained automotive grade AA5754-O aluminum alloy were evaluated to get insight into the role of amount and direction of uni-axial pre-strain. The following are the major conclusions.

(a) The yield strength of the AA5754-O aluminum alloy sheet metals increased with simultaneous decrease in the % total elongation due to strain hardening. The true stress-strain responses obtained from uni-axial tensile and stack compression tests of as-received and pre-strained materials were lying in a band, and the results were found to match reasonably with the Hollomon isotropic hardening law.

(b) The Yld96 anisotropy plasticity theory was applied to evaluate the anisotropy coefficients of as-received and pre-strained materials successfully. A very negligible distortion in yield loci of all the pre-strained materials was observed in the normalized stress space. Also, the Hollomon isotropic hardening law in-conjunction with the Yld96 anisotropy model of the as-received material could able to predict the yield evolution of all pre-strained materials close to the experimental data.

(c) The forming limit strains of the pre-strained materials were found to shift depending on the amount and direction of uni-axial pre-strain. The shift was towards the tension-compression region with the increase in the limiting strains in the case of transverse direction (TD) pre-strained materials. However, the limiting strains decreased with a shift towards the tension-tension region for rolling direction (RD) pre-strained materials.

(d) The σ-FLD was estimated from ε-FLD of the as-received AA5754-O sheet material using the Yld96 anisotropy constitutive equation in-conjunction with the Hollomon power hardening law. Moreover, the dynamic shift of ε-FLDs was estimated by decoupling the σ-FLD using the Yld96 plasticity theory within a root mean square error of 0.008.

(e) The FE model of both the uni-axial pre-straining and subsequent out-of-plane stretch forming process were developed, and the formability behavior in terms of LDH, thickness distribution and maximum thinning location were predicted successfully using the σ-FLD of as-received material. This will help the sheet metal stamping industries to save energy, material and effort by avoiding the evaluation of tensile properties and ε-FLDs at each stage of the pre-strain.

(f) It was found that the LDH of the AA5754-O alloy decreased with the increase in the pre-strain, but the effect of direction of uni-axial pre-strain was very negligible. The thickness distributions with the maximum thinning location were significantly affected by the amount of pre-strain. It was observed that the maximum thinning location shifted very close to the pole in the case of 12.2 % pre-strained materials.

Funding: This research did not receive any specific grant from funding agencies in the public, commercial, or not-for-profit sectors.

References

[1] Pourboghrat F, Venkatesan S, Carsley JE. LDR and hydroforming limit for deep drawing of AA5754 aluminum sheet. Journal of Manufacturing Processes. 2013 Oct 31;15(4):600-15.

[2] Hazra S, Williams D, Roy R, Aylmore R, Smith A. Effect of material and process variability on the formability of aluminium alloys. Journal of Materials Processing Technology. 2011 Sep 30;211(9):1516-26.

[3] Narasimhan K, Miles MP, Wagoner RH. A better sheet-formability test. Journal of Materials Processing Technology. 1995 Mar 31;50(1):385-94.

[4] Kacem A, Krichen A, Manach PY, Thuillier S, Yoon JW. Failure prediction in the hole-flanging process of aluminium alloys. Engineering Fracture Mechanics. 2013 Feb 28;99:251-65.

[5] Tekıner Z. An experimental study on the examination of springback of sheet metals with several thicknesses and properties in bending dies. Journal of Materials Processing Technology. 2004 Jan 1;145(1):109-17.

[6] Harpell ET, Worswick MJ, Finn M, Jain M, Martin P. Numerical prediction of the limiting draw ratio for aluminium alloy sheet. Journal of Materials Processing Technology. 2000 Apr 3;100(1):131-41.

[7] Demirci HI, Esner C, Yasar M. Effect of the blank holder force on drawing of aluminum alloy square cup: Theoretical and experimental investigation. Journal of Materials Processing Technology. 2008 Sep 12;206(1):152-60.

[8] Kotkunde N, Deole AD, Gupta AK, Singh SK. Comparative study of constitutive modeling for Ti–6Al–4V alloy at low strain rates and elevated temperatures. Materials & Design. 2014 Mar 31;55:999-1005.

[9] Moshksar MM, Mansorzadeh S. Determination of the forming limit diagram for Al 3105 sheet. Journal of Materials Processing Technology. 2003 Oct 1;141(1):138-42.

[10] Harrison NR, Friedman PA, Pan J. Warm forming die design, Part III: Design and validation of a warm forming die. Journal of Manufacturing Processes. 2015 Oct 31;20:356-66.

[11] Panicker SS, Singh HG, Panda SK, Dashwood R. Characterization of tensile properties, limiting strains, and deep drawing behavior of AA5754-H22 sheet at elevated temperature. Journal of Materials Engineering and Performance. 2015 Nov 1;24(11):4267-82.

[12] Wilson JF, Kinsey BL, Korkolis YP. Development of a biaxial loading frame for sheet metal. Journal of Manufacturing Processes. 2013 Oct 31;15(4):580-5.

[13] Gupta AK, Kumar DR. Formability of galvanized interstitial-free steel sheets. Journal of Materials Processing Technology. 2006 Feb 28;172(2):225-37.
[14] Kim M, Rickhey F, Lee H, Kim N. Analytical determination of forming limit curve for zirlo and its experimental validation. Journal of Manufacturing Processes. 2016 Aug 31;23:122-9.
[15] Ma B, Diao K, Wu X, Li X, Wan M, Cai Z. The effect of the through-thickness normal stress on sheet formability. Journal of Manufacturing Processes. 2016 Jan 31;21:134-40.
[16] Yoshida T, Katayama T, Usuda M. Forming-limit analysis of hemispherical-punch stretching using the three-dimensional finite-element method. Journal of Materials Processing Technology. 1995 Mar 31;50(1):226-37.
[17] Marciniak Z, Kuczyński K. Limit strains in the processes of stretch-forming sheet metal. International Journal of Mechanical Sciences. 1967 Sep 1;9(9):609IN1613-12IN2620.
[18] Stören S, Rice JR. Localized necking in thin sheets. Journal of the Mechanics and Physics of Solids. 1975 Dec 1;23(6):421-41.
[19] Hussaini SM, Krishna G, Gupta AK, Singh SK. Development of experimental and theoretical forming limit diagrams for warm forming of austenitic stainless steel 316. Journal of Manufacturing Processes. 2015 Apr 30;18:151-8.
[20] Tisza M, Kovács ZP. New methods for predicting the formability of sheet metals. Journal of Production Processes and Systems. 2012;6(1):45-54.
[21] Conrad H. Effect of the strain-rate sensitivity of the flow stress on the stretch formability of sheet metals. Journal of Mechanical Working Technology. 1978 Aug 31;2(1):67-74.
[22] Bressan JD. The influence of material defects on the forming ability of sheet metal. Journal of Materials Processing Technology. 1997 Dec 1;72(1):11-4.
[23] Narayanan RG, Narasimhan K. Influence of the weld conditions on the forming-limit strains of tailor-welded blanks. The Journal of Strain Analysis for Engineering Design. 2008 Apr 1;43(4):217-27.
[24] Gutscher G, Wu HC, Ngaile G, Altan T. Determination of flow stress for sheet metal forming using the viscous pressure bulge (VPB) test. Journal of Materials Processing Technology. 2004 Feb 15;146(1):1-7.
[25] Laukonis JV, Ghosh AK. Effects of strain path changes on the formability of sheet metals. Metallurgical Transactions A. 1978 Dec 1;9(12):1849-56.

[26] Graf AF, Hosford WF. Calculations of forming limit. Metallurgical Transactions A. 1993 Nov 1;24(11):2497-501.
[27] Stoughton TB. A general forming limit criterion for sheet metal forming. International Journal of Mechanical Sciences. 2000 Jan 31;42(1):1-27.
[28] Bandyopadhyay K, Basak S, Panda SK, Saha P. Use of stress based forming limit diagram to predict formability in two-stage forming of tailor welded blanks. Materials & Design. 2015 Feb 15;67:558-70.
[29] Hasan RZ, Kinsey BL, Tsukrov I. Effect of element types on failure prediction using a stress-based forming limit curve. Journal of Manufacturing Science and Engineering. 2011 Dec 1;133(6):061002.
[30] Basak S, Bandyopadhyay K, Panda SK, Saha P. Prediction of formability of bi-axial pre-strained dual phase steel sheets using stress-based forming limit diagram. In: Narayanan RG, Dixit US, editors. Advances in material forming and joining, Springer India; 2015, p. 167-192.
[31] Basak S, Panda SK, Zhou YN. Formability assessment of prestrained automotive grade steel sheets using stress based and polar effective plastic strain-forming limit diagram. Journal of Engineering Materials and Technology. 2015 Oct 1;137(4):041006.
[32] ASTM E. 517-00. Standard test method for plastic strain ratio R for sheet metal. Philadelphia: American Society for Testing and Materials. 2006.
[33] Vial C, Hosford WF, Caddell RM. Yield loci of anisotropic sheet metals. International Journal of Mechanical Sciences. 1983 Dec 31;25(12):899-915.
[34] Tari DG, Worswick MJ, Ali U, Gharghouri MA. Mechanical response of AZ31B magnesium alloy: experimental characterization and material modeling considering proportional loading at room temperature. International Journal of Plasticity. 2014 Apr 30;55:247-67.
[35] Barlat F, Maeda Y, Chung K, Yanagawa M, Brem JC, Hayashida Y et al. Yield function development for aluminum alloy sheets. Journal of the Mechanics and Physics of Solids. 1997 Dec 31;45(11):1727-63.
[36] Banabic D. Formability of metallic materials: plastic anisotropy, formability testing, forming limits. 1st ed. Springer Science & Business Media; 2000 Nov 29.
[37] Abedrabbo N, Pourboghrat F, Carsley J. Forming of aluminum alloys at elevated temperatures–Part 1: Material characterization. International Journal of Plasticity. 2006 Feb 28;22(2):314-41.

[38] Rees, D. W. A. Sheet orientation and forming limits under diffuse necking. Applied Mathematical Modelling 1996, 20, no. 8: 624-635.
[39] Stoughton, T.B., Yoon, J.W. Sheet metal formability analysis for anisotropic materials under non-proportional loading. International Journal of Mechanical Sciences, 2005, 47(12), pp.1972-2002.
[40] Hariharan, K., Nguyen, N.T., Barlat, F., Lee, M.G., Kim, J.H. A pragmatic approach to accommodate in-plane anisotropy in forming limit diagrams. Mechanics Research Communications, 2014, 62, pp.5-17.

List of figures

List of tables

Vitae

S. Dhara

Mr. Sisir Dhara received his M. Tech degree in Manufacturing Science and Engineering from Department of Mechanical Engineering, IIT Kharagpur, India. He gained his B. Tech degree in Production Engineering Department from Jadavpur University, Kolkata, India. His research interests are sheet metal forming processes, theory of plasticity, finite element modeling of sheet metal forming processes and formability evaluation of sheet metal used in automotive industry.

S. Basak

Mr. Shamik Basak received his B.E. in Mechanical Engineering from Jadavpur University, India and M. Tech. in Manufacturing Science and Engineering from Department of Mechanical Engineering, IIT Kharagpur, India. He worked in Indian Space Research Organization in the area of launch vehicle integration, solid motor and satellite preparation in launch pad area. He is presently working as a Ph.D. Scholar in IIT Kharagpur, India. His research interests are formability and failure analysis of sheet metals, theory of plasticity, friction stir welding, laser material processing and application of finite element methods in sheet metal forming processes.

S. K. Panda

Dr. Sushanta Kumar Panda is presently working as Associate Professor in the Department of Mechanical Engineering, IIT Kharagpur, India. He received his PhD from the Department of Mechanical Engineering, IIT Delhi, India and further worked as Postdoctoral fellow in the Center for Advanced Materials Joining, University of Waterloo, Canada before joining in IIT Kharagpur. His research interests are sheet metal forming processes, sheet and tube hydro forming, formability testing design and development, plasticity for metal deformation modeling and simulation and friction stir processing of sheet metal.

S. Hazra

Dr Sumit Hazra is presently the Senior Research Fellow at WMG, University of Warwick, UK. He joined the Premium Automotive R&D Program based in WMG. He received his

undergraduate and postgraduate degrees from the Mechanical Engineering Department of Imperial College, London. His research interests are characterizing subtle defects on cosmetic surfaces and identifying their causes, predicting the forming limits of sheet metal, understanding the effect of material and process variability on the formability of aluminum sheet material, measurement of residual stresses in sheet metals and the fracture of polymers under impact loading etc.

B. Shollock

Professor Barbara Shollock is presently the Academic Director of WMG, University of Warwick, UK and Professor at the Steels Processing research group, WMG, University of Warwick, UK. She joined WMG from Imperial College, London where she was a Senior Lecturer. She received her PhD from University of Oxford. She was a TFR visiting Professor at Technical University of Lulea Sweden and held an industrial fellowship with The Royal Society. Her research interests are high temperature stability in nickel superalloys, precipitation in aluminum alloys, long term stability of the microstructure and coatings micro-mechanisms of deformation in aluminum, titanium and nickel alloys.

R. Dashwood

Professor Richard Dashwood is currently the *Deputy Vice-Chancellor Research of* Coventry University, UK and Professor of Engineering Materials, Coventry University, UK. He joined Coventry University in early 2016 from WMG, Warwick University, where he was Academic Director and Director of Research of WMG, Chief Technical Officer of WMG's High Value Manufacturing Catapult and was head of the engineering materials and electrochemical engineering research groups, WMG. He received his PhD from the Department of Materials Science and Engineering, Imperial College, London. His research interests are thermo-mechanical processing, sheet metal forming, design and development of lightweight structures in automobiles and electrochemical engineering.